Extreme Warming in the Kara Sea and Barents Sea during the Winter Period 2000–16

SVENJA H. E. KOHNEMANN AND GÜNTHER HEINEMANN

Environmental Meteorology, University of Trier, Trier, Germany

DAVID H. BROMWICH

Polar Meteorology Group, Byrd Polar and Climate Research Center, The Ohio State University, Columbus, Ohio

OLIVER GUTJAHR

Max Planck Institute for Meteorology, Hamburg, Germany

(Manuscript received 26 September 2016, in final form 28 July 2017)

ABSTRACT

The regional climate model COSMO in Climate Limited-Area Mode (COSMO-CLM or CCLM) is used with a high resolution of 15 km for the entire Arctic for all winters 2002/03–2014/15. The simulations show a high spatial and temporal variability of the recent 2-m air temperature increase in the Arctic. The maximum warming occurs north of Novaya Zemlya in the Kara Sea and Barents Sea between March 2003 and 2012 and is responsible for up to a 20°C increase. Land-based observations confirm the increase but do not cover the maximum regions that are located over the ocean and sea ice. Also, the 30-km version of the Arctic System Reanalysis (ASR) is used to verify the CCLM for the overlapping time period 2002/03–2011/12. The differences between CCLM and ASR 2-m air temperatures vary slightly within 1°C for the ocean and sea ice area. Thus, ASR captures the extreme warming as well. The monthly 2-m air temperatures of observations and ERA-Interim data show a large variability for the winters 1979–2016. Nevertheless, the air temperature rise since the beginning of the twenty-first century is up to 8 times higher than in the decades before. The sea ice decrease is identified as the likely reason for the warming. The vertical temperature profiles show that the warming has a maximum near the surface, but a 0.5°C yr^{-1} increase is found up to 2 km. CCLM, ASR, and also the coarser resolved ERA-Interim data show that February and March are the months with the highest 2-m air temperature increases, averaged over the ocean and sea ice area north of 70°N; for CCLM the warming amounts to an average of almost 5°C for 2002/03–2011/12.

1. Introduction

During 1989–2008, the near-surface temperature increase of the ECMWF interim reanalysis (ERA-I) data is 0.5°C $decade^{-1}$ for summer and 1.6°C $decade^{-1}$ for the winter season averaged over the Arctic (Screen and Simmonds 2010; Overland and Wang 2010). The Intergovernmental Panel on Climate Change Fifth Assessment Report (IPCC 2013) projects a further warming for the central Arctic of 3°–4°C over the next 50 years, based on different emissions scenarios and a large number of different climate models. The Arctic warming occurs during the entire year, but has its maximum in autumn and winter (Cohen et al. 2014).

The warming, approximately twice as strong in the Arctic than in the global mean, is also known as "Arctic amplification" (Serreze and Francis 2006; Serreze et al. 2009; Screen and Simmonds 2010; Cowtan and Way 2014). It is supposed to be caused by a wide range of physical processes. Most of them are strongly coupled with the decreasing sea ice area (e.g., Lindsay et al. 2009; Comiso 2012; Stroeve et al. 2012) since the late 1970s partly due to human-induced global warming (IPCC 2013; Notz and Marotzke 2012). Contributing processes include (i) shortwave albedo change (Winton 2006;

Denotes content that is immediately available upon publication as open access.

Corresponding author: Svenja H. E. Kohnemann, kohnemann@uni-trier.de

DOI: 10.1175/JCLI-D-16-0693.1

Serreze et al. 2009; Serreze and Barry 2011; Screen et al. 2012), (ii) changes of the aerosol concentration and the deposits of black carbon on the Arctic surfaces (Shindell and Faluvegi 2009), (iii) water vapor and cloud cover changes (Francis and Hunter 2006; Graversen and Wang 2009), (iv) increasing greenhouse gas forcing (Stroeve et al. 2012; Gillett et al. 2008), (v) temperature or Planck feedback (Pithan and Mauritsen 2014), and also (vi) changing poleward transport of heat and moisture into the Arctic (Graversen et al. 2008). Several studies also investigate the linkages between midlatitude extreme weather, storm tracks, planetary waves, and the jet stream. Cohen et al. (2014) provide an overview article about the different linkages, concluding that an improved process understanding is still needed. A close analysis of the regional and temporal variability of the Arctic warming helps to advance the understanding of the influences of Arctic amplification.

However, estimations about the temperature increase and the understanding of regional and seasonal temperature changes in the Arctic are hindered by the fact that long-term in situ measurements do not exist for vast areas of the Arctic. Simmons and Poli (2015) show that the conventional meteorological observational coverage for radiosondes from 70° to 90°N is variable on a low frequency and decreases between 1989 and 1996 but has partially recovered till 2012. The decline in radiosonde observations for the Arctic is in contrast to the increasing number of radiosondes on a global scale (Simmons and Poli 2015). The number of synoptic stations has increased for Greenland and northernmost Canada but declined in Russia in the 1990s and has only partly recovered afterward. Because of a change from manual to automatic stations the number of available surface observations increased each year (Simmons and Poli 2015) but is still sparse. The observational coverage over ocean and sea ice is even lower and there are only data from buoys, ice stations, or field experiments available. Some satellite measurements (e.g., MODIS) improve the availability of data over sea ice (Simmons and Poli 2015).

A different approach is the use of mesoscale atmospheric models and reanalyses to analyze the temporal and regional developments. Reanalyses have the advantage that they assimilate observations to keep simulations close to reality. A comparison of global reanalysis datasets for the Arctic is presented by Lindsay et al. (2014). With regard to the 2-m air temperature, the study shows that deviations are small for the Climate System Forecast Reanalysis (CFSR), the Modern-Era Retrospective Analysis for Research and Applications (MERRA), the ERA-I, and the Japanese 25-year Reanalysis Project (JRA-25) for the land regions of

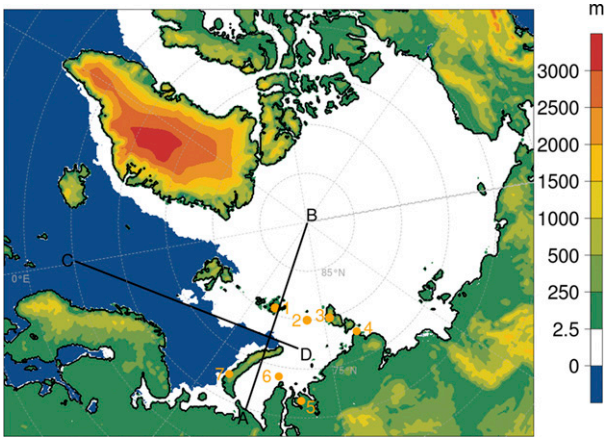

FIG. 1. CCLM 15-km model domain and the surface height. The orange points mark the locations of the seven observational stations in the Kara Sea and Barents Sea (see Table 1). (Straight black lines indicate cross sections shown in Fig. 8.) Blue color indicates water and white is the sea ice area for 8 Apr 2014.

Europe, Siberia, and North America for the time period of 1980–2009. In particular, ERA-I has small biases, is closely correlated to the observations and has a high consistency. Simmons and Poli (2015) argue that ERA-I agrees well with measured surface air temperature data but has warm winter biases over the sea ice. Global reanalyses have the disadvantage of a coarse resolution. The newly developed Arctic System Reanalysis (ASR; Byrd Polar and Climate Research Center) has a higher horizontal resolution (30 km; Bromwich et al. 2012) than previous reanalyses covering the Arctic. ASR is also specially adapted for the Arctic region and thus Bromwich et al. (2016) could show that ASR is in good agreement with observed 2-m air temperatures, with the annual biases being smaller in comparison to ERA-I for December 2006–November 2007.

In the present study, the nonhydrostatic, regional climate model COSMO in Climate Limited-Area Mode (COSMO-CLM or CCLM) is used with a horizontal resolution of 15 km for the Arctic in the winter seasons 2002/03–2014/15 (Fig. 1). CCLM (Rockel et al. 2008) is based on the COSMO Model being used for operational weather forecasting (Steppeler et al. 2003). For the Arctic, a thermodynamic sea ice model was implemented in COSMO (Schröder et al. 2011) in CCLM and in CCLM by Gutjahr et al. (2016). This configuration was already used in previous studies in the Arctic. In Schröder et al. (2011) a verification of the COSMO Model was performed using four automatic weather stations over sea ice in the Laptev Sea area, and very good agreement was found. In addition, a comparison with MODIS-based surface temperatures shows that the mean value of the surface temperature differs by just

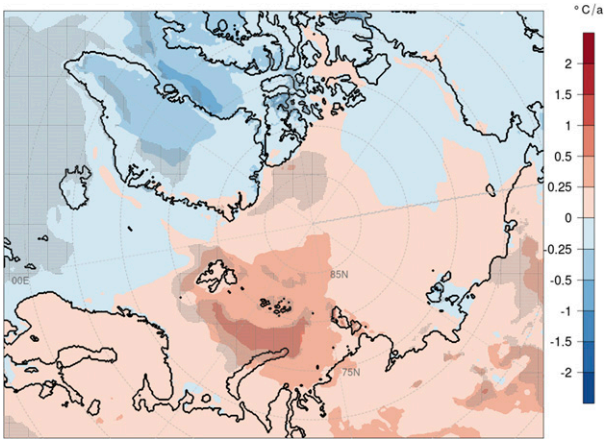

FIG. 2. CCLM 2-m air temperature trends (°C yr^{-1}) for the winter mean (November–April) 2002/03–2011/12. Gray shaded regions indicate significant grid boxes at a 95% level.

0.2 K (Schröder et al. 2011). Ebner et al. (2011) used the COSMO Model for studies of the impact of polynyas on the atmospheric boundary layer. Further, sea ice production rates for the Laptev Sea were calculated with COSMO Model simulations in Bauer et al. (2013). Recently Gutjahr et al. (2016) used CCLM to quantify the sea ice production in the same region and investigate its sensitivity to the assumptions of thin-ice thickness in the tile approach. The comparison of these results with automatic weather stations over sea ice shows that CCLM is able to reproduce the observed near-surface variables (temperature bias of around −1°C). We study mainly the spatial variability and the monthly temporal variations of the Arctic air temperature increase since the beginning of the twenty-first century, but with focus on the CCLM simulation period. CCLM simulations are verified with the 30-km version of the ASR data and with land-based observations. The regional focus is on the Kara Sea and Barents Sea area, because the largest warming is found in these regions (Fig. 2).

2. Methods and datasets

a. CCLM

The nonhydrostatic regional climate model CCLM (version v5.0_clm1; Rockel et al. 2008), was used for the Arctic winter periods (November–April) from 2002/03 to 2014/15. The model was run in a forecast mode for daily forecast simulations including a spinup time of 6 h in order to keep the simulations close to reality (each run covers 30 h). No observations were assimilated during the runs. ERA-I data (Dee et al. 2011) were used as initial and boundary data. No spectral nudging was performed.

The horizontal resolution is 15 km for a 450 × 350 gridpoint domain, covering the whole Arctic (Fig. 1). The model has 42 vertical sigma levels up to 22 km, of which 16 are below 2-km height. The model equations are based on the primitive thermo-hydrodynamical equations and solved on an Arakawa C/Lorenz grid applied on a rotated spherical coordinate system. The daily ice situation is prescribed by a combination of different datasets. On the one side, the Advanced Microwave Scanning Radiometer for Earth Observing System (AMSR-E onboard *Aqua*) and AMSR-2 [onboard the *Global Change Observation Mission for Water–1* (*GCOM-W1*); Spreen et al. 2008, provided by the University of Bremen] data are used for sea ice concentration and on the other side the sea ice thickness is taken from the Pan-Arctic Ice–Ocean Modeling and Assimilation System (PIOMAS; Zhang and Rothrock 2003). Compared to the standard CCLM version, several adaptations were made (Gutjahr et al. 2016). Over sea ice the thermodynamic two-layer sea ice model of Schröder et al. (2011) is used. Thin ice (≤20 cm) is considered to be free of snow, sea ice thicker than 20 cm is defined to have a snow cover of 10 cm (Schröder et al. 2011). The roughness length for sea ice is taken as 1 cm and a modified Charnock formula (Doms et al. 2011) is applied for open water areas. Surface energy fluxes for fractional ice cover are calculated by a tile approach, and a sea ice albedo scheme after Koltzow (2007) is used (Gutjahr et al. 2016).

b. Reanalyses and observations

The ASR is a regional reanalysis covering the Arctic and midlatitudes (poleward of 40°N) and was developed with the purpose of a better understanding of the processes and consequences of a changing Arctic climate system (Bromwich et al. 2012). The ASR is based on the high-resolution, nonhydrostatic Polar Weather Research and Forecasting Model (Polar WRF, version 3.3.1) with ERA-I data used as lateral boundary conditions. ASR has a horizontal resolution of 30 km [2000–12; version 1 (ASRv1)] and 15 km [2000–12; version 2 (ASRv2), completed early 2017, but it was not ready for this manuscript], with 71 vertical levels. A wide variety of observations (details below) are assimilated using three-dimensional variational data assimilation. It features a comprehensive sea ice description similar to that used by CCLM. As a result, ASRv1 data provide a valuable mesoscale dataset of the Arctic atmosphere–sea ice–land surface system for the period 2000–12 at 3-h intervals (Bromwich et al. 2016), and are used here.

ERA-I (Dee et al. 2011) is a global reanalysis with a horizontal resolution of approximately 79 km with 60 levels in the vertical and spans from 1979 to the present

at 6-h intervals. It features coupled atmosphere and land surface models with specified ocean conditions. The sea ice description is much simpler than that used by CCLM and ASR. ERA-I uses four-dimensional data assimilation to incorporate many of the conventional observations used by ASR and emphasizes the use of a vast array of satellite data. ERA-I was the best performing global reanalysis over the Arctic among the seven evaluated by Lindsay et al. (2014).

The Arctic Ocean is a data-sparse, but not data-void, region for reanalyses. Both reanalyses assimilate conventional (surface and upper air) observations from the land areas surrounding, and from islands within, the Arctic Ocean. Atmospheric advection via the short-term model forecast that serves as the basis for assimilation can move information from data-rich areas to the more data-sparse sea ice zone. The surface pressure data from buoys drifting in the sea ice are also included. Satellite and aircraft observations are assimilated. Therefore, although the reanalyses are less constrained than the adjacent land areas, they are far from pure model forecasts. Further constraint is provided by sea ice concentration specified from satellite passive microwave observations.

A comprehensive verification of ASRv1 and ERA-I has been conducted for the Arctic and moderate latitudes by Bromwich et al. (2016). They show that ASRv1 is a high-quality reanalysis dataset with accurate results in the surface variables with the greatest advances over ERA-I in near-surface temperature, moisture, and wind. Upper-level comparisons show improvements over ERA-I in relative humidity and wind speed throughout the troposphere. The forecast clouds, precipitation, and the surface radiation perform less well than ERA-I, with the microphysical scheme also showing some inaccuracies (Wesslen et al. 2014) that have been alleviated in ASRv2.

ASR does a better job identifying extreme cyclones over the Arctic Ocean than other global reanalyses including ERA-I (Tilinina et al. 2014). A much higher percentage of polar lows in the northern North Atlantic are captured by ASR than ERA-I (Smirnova and Golubkin 2017). The ASR data have been subject of several topographically forced wind studies (Moore 2013; Moore et al. 2015, 2016) that mostly demonstrate its better performance than ERA-I.

For the comparison between ASR and CCLM, the ASR data are bilinear interpolated to the CCLM grid for winters (November–April) 2002/03–2011/12. Hourly CCLM data are sampled every third time step, in order to enable a better comparison with the 3-hourly ASR data. ERA-I data are used with their 6-hourly resolution (Dee et al. 2011). Monthly means are generally the basis for all analyses, except for some correlation calculations between the meteorological stations and CCLM and the percentile calculations of daily extremes. For the comparison with meteorological surface stations, the four closest grid boxes are interpolated to the location of each station for CCLM, ASR, and ERA-I. Only stations with more than 75% coverage are used. The meteorological surface stations are part of the World Meteorological Organization's observing network.

Trends are calculated with linear regression using an ordinary least squares method. Statistical significances are calculated using the Student's t test at the 95% and 99% confidence levels. The calculations of the coefficients of determination is based on Pearson's correlations. Time series were not detrended for the analysis.

3. Results: Near-surface temperature validation

a. Comparison with observational data

Verifying CCLM simulations in the Arctic is challenging because of the lack of measurements, especially over the ocean and sea ice area. Regarding the region of interest, the Barents Sea and Kara Sea around Novaya Zemlya, seven meteorological stations are located there (for locations see Fig. 1). Table 1 shows the statistical analysis for the 2-m air temperature of these stations in comparison with the monthly averaged CCLM and ASR data for the winters (November–April) 2002/03–2011/12 [except observation station 1 (Polar GMO), which only provides data for January 2004–December 2012]. The CCLM 2-m air temperature is not directly simulated, but computed between the skin temperature and temperature at the lowest model level (20 m) using surface layer similarity theory. In contrast, the ASR 2-m air temperatures are calculated from the observed 2-m air temperatures and temperatures at the lowest model level of Polar WRF at 4 m. As a consequence, the ASR 2-m air temperatures are not independent from the observations (Bromwich et al. 2016). Therefore, biases and RMSEs are generally smaller for ASR. Correlation coefficients for ASR monthly mean 2-m air temperature exceed 0.98. The correlation coefficients of CCLM and the seven stations range between 0.94 and 0.97 on a monthly mean basis. The CCLM coefficients of determination for daily means lie between 0.92 and 0.98 for the stations located in the region of interest (Fig. 3). The comparison between CCLM and 88 stations (located in the CCLM domain below a height of 50 m, with a total coverage of at least 75% of the data) shows that CCLM performs very well for most regions in the Arctic, especially along the Siberian coast ($\geq$0.92). The biases for CCLM range between a smaller cold bias of -0.7°C up to a warm bias of 1.3°C for the seven synoptic stations (Table 1). ASR biases vary between -0.8° and 1.1°C. In the regional comparison to

TABLE 1. Statistical comparison of monthly means (bias, RMSE, and correlation coefficients) between station data (OBS) and CCLM and ASR for all winter periods 2002/03–2011/12.

Station				Mean			Bias		RMSE		r	
No.	Name (WMO No.)	Lat	Lon	OBS	CCLM	ASR	CCLM	ASR	CCLM	ASR	CCLM	ASR
1	Polar GMO im. E.T. Krenkelja (20046)[a]	80.62°N	58.05°E	−16.10	−15.20	−16.30	0.90	−0.21	1.81	0.74	0.95	0.99
2	Ostrov Vize (20069)	79.48°N	76.99°E	−19.22	−18.36	−18.57	0.86	0.64	1.72	0.92	0.97	0.99
3	Golomjannyj (20087)	79.55°N	90.57°E	−21.92	−20.74	−20.94	1.17	0.98	2.13	1.33	0.94	0.99
4	GMO im. E.K. Federova (20292)	77.72°N	104.3°E	−22.77	−23.48	−22.75	−0.71	0.02	1.81	0.89	0.96	0.98
5	Ostrov Dikson (20674)	73.5°N	80.4°E	−19.82	−19.07	−18.70	0.75	1.12	1.52	1.3	0.97	0.99
6	im. M.V. Popova (20667)	73.33°N	70.05°E	−17.91	−16.59	−16.85	1.33	1.07	1.88	1.3	0.97	0.99
7	Malye Karamakuly (20744)	72.37°N	52.7°E	−9.43	−10.02	−10.26	−0.59	−0.83	1.03	0.97	0.97	0.99
All station mean				−18.17	−17.64	−17.77	0.53	0.40	1.70	1.06	0.96	0.99

[a] Only for the years 2004–12.

the 88 station data, also the other biases around the Siberian coast are very small (from −2.5° to 2.0°C) for CCLM (Fig. 3). The regional analysis shows that CCLM is generally slightly warmer than the measured data (from −0.5° to 2°C) for the Kara Sea and Barents Sea region, but slightly cooler for other regions in Siberia. Greenland and northern Norway show higher cold biases ranging between −1.3° and −4.9°C and are caused by highly variable topography. Especially in the region of interest, the good accordance between CCLM and observations indicates a high quality of the CCLM monthly means but also of the daily mean 2-m air temperatures.

To have a closer analysis at the temporal performance, Fig. 4 compares the March averages from the 2-m air temperature observations of station 2 (Ostrov Vize, WMO No. 200690; 1955–2017) with the 2-m air temperature of CCLM (2003–15), ASR (2000–12), and ERA-I (1979–2016). The station is located at the eastern edge of the area with maximum warming (see Fig. 2). The differences between the observations, the modeled data, and the reanalyses are mainly below 2°C. Thus, the comparison reveals that the near-surface air temperature is well captured by the model datasets during the period. Just as in Table 1, a slightly better agreement is seen between ASR data and the observed temperatures. The same is true for the other six stations in the region of interest and the other five winter months (not shown). Averaged over all seven synoptic stations, differences in the monthly 2-m air temperature biases are small (Fig. 4). CCLM has the smallest bias in December with 0.2°C and the highest biases in March with 1.4°C. The calculated biases for all 88 stations for March (not shown) are in general around 1°C, which is slightly larger than the mean for all winter months (Fig. 3). Comparing the different datasets, ERA-I shows generally the highest biases in all months and ASR shows the smallest ones. Furthermore, Fig. 4 shows that the trends of the data are highly dependent on the time period as a result of a high interannual variability of the 2-m air temperature. Differences of 5°C and more between sequential years are a common feature. Thus, the increase of the observed 2-m air temperature in March is only 1.2°C decade^{-1} for the 62-yr period, but the increases for the last decades are considerably higher, which is also reflected by the model data. ERA-I shows an increase of 2.3°C decade^{-1} for the period of 1979–2016. ASR increases by 6.8°C decade^{-1} for 2000–12 and CCLM increases by 9.2°C decade^{-1} for 2003–15. In comparison, the ERA-I trend for the ASR time period (2000–12) is 7.5°C decade^{-1} and for the CCLM period (2003–15) the ERA-I trend amounts to 9.0°C decade^{-1}. The increase for the CCLM grid cell with the maximum warming over sea ice is clearly stronger with a trend of 12.4°C decade^{-1} for March 2003–15 (for exact location see the March point in Fig. 7).

We compared CCLM surface temperatures with MODIS surface temperatures (Preußer et al. 2016) in the Kara Sea. Differences of the area-average between CCLM and MODIS monthly means for March 2003–15 range between −4° and +1.6°C (not shown). The mean temperatures are −19.2°C for CCLM and −17.9°C for MODIS (i.e., CCLM is −1.3°C colder than MODIS). However, this difference is within the uncertainty of the MODIS sea ice temperature product (Hall et al. 2004). The MODIS data show also a warming of 3.9°C decade^{-1}, which is significantly smaller than the CCLM trend of 7.2°C decade^{-1} for this region. But it has to be noted that a comparison with MODIS is biased to cloud-free conditions and that the trend calculation could be performed for only 50% of the area because of the cloudy conditions.

b. *Comparison of ASR and CCLM for the Arctic*

The 2-m air temperatures for CCLM and ASR only differ within the small range of ±0.5°C over sea ice for all winters (not shown). The differences over land are larger,

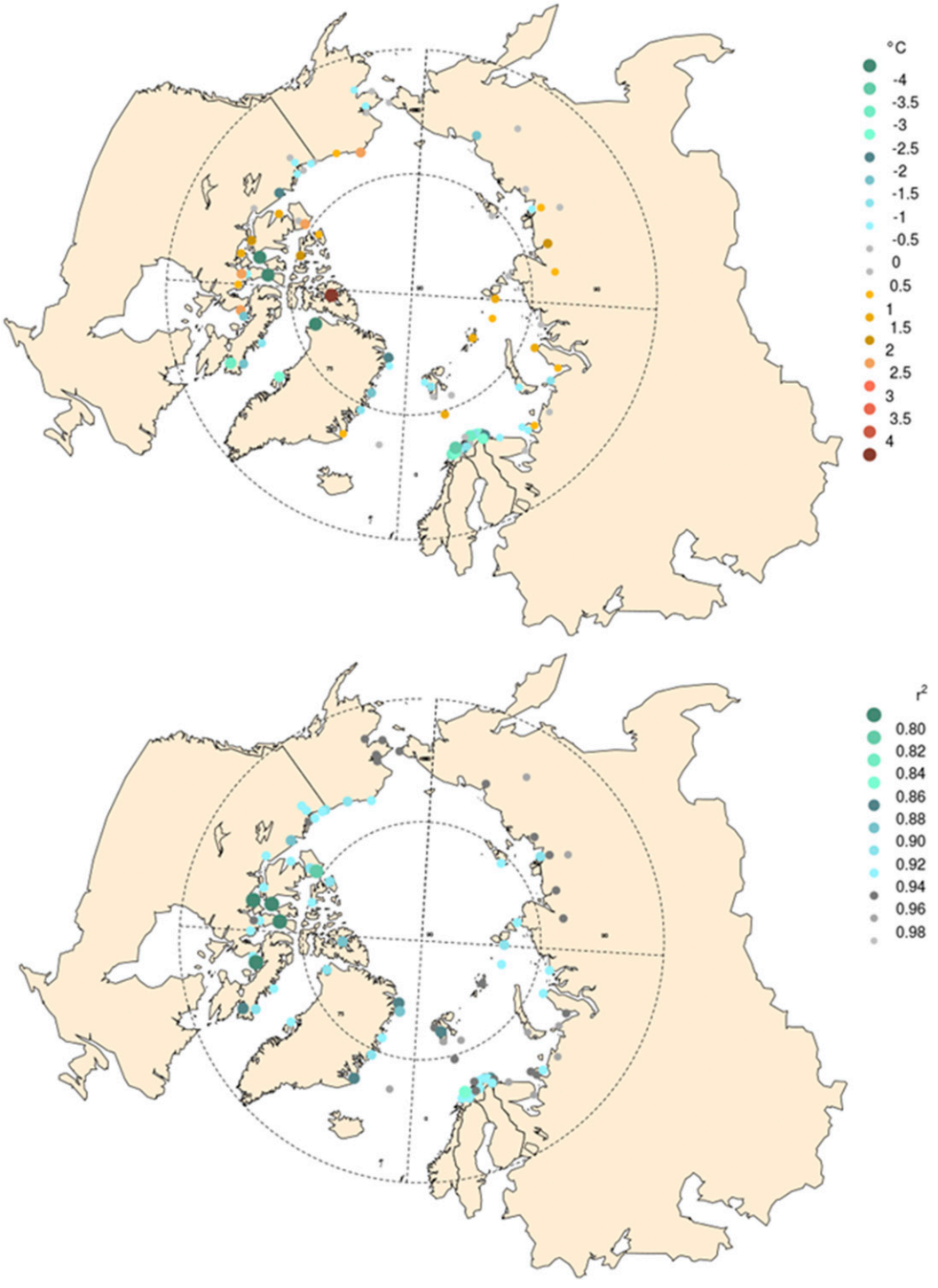

FIG. 3. (top) The 2-m air temperature bias (CCLM minus observation) and (bottom) coefficient of determination based on daily means for CCLM and all synoptic stations located below 50-m height in the CCLM domain for the winter periods (November–April) 2002/03–2011/12.

for example, because of using different land surface representations and soil models. Larger disagreement between CCLM and ASR is found for the 95th and 99th percentiles of the daily mean 2-m air temperatures (Fig. 5).

For the whole period, it can be seen that the extremes in daily mean temperatures are above the freezing point over the ocean and below 0°C over sea ice and land areas (Figs. 5a,b). The regional patterns of the 95 and the 99

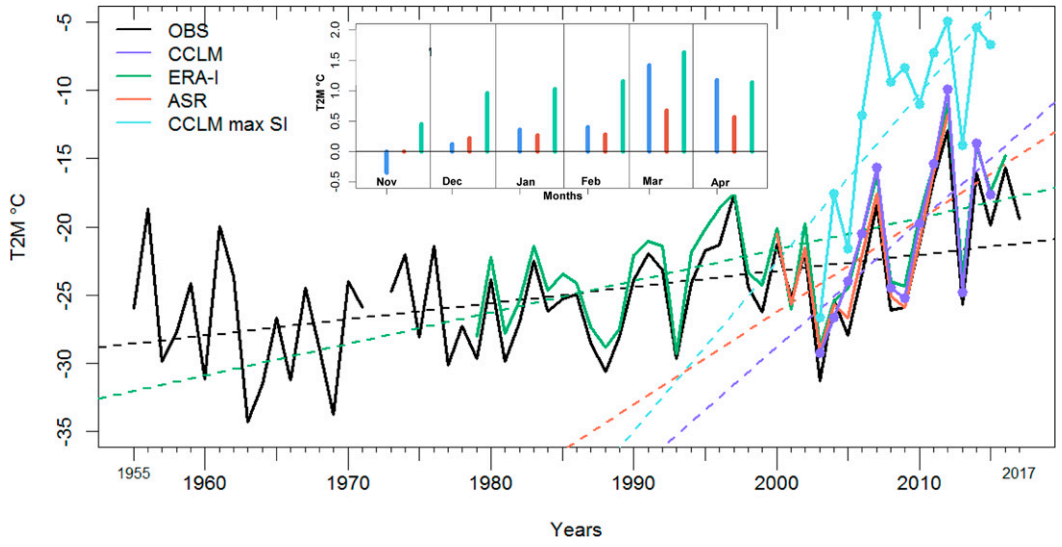

FIG. 4. Time series of the 2-m air temperature for Ostrov Vize (OBS; black) and related gridbox 2-m air temperature of CCLM (dark blue), ERA-I (green), and ASR (red) for March monthly means. The light blue line (CCLM max SI) is the March period of CCLM grid box with the max 2-m air temperature over sea ice (77.40°N, 60.59°E or see the March point in Fig. 7). Dashed lines present the linear trends. The inset chart shows 2-m air temperature biases (e.g., CCLM minus observation) for all seven stations in the region of interest for the six winter months (November–April) 2002/03–2011/12.

distributions are very similar. The lowest values occur over Greenland and the sea ice regions of Canada and Greenland. The warmest regions are located in the Atlantic Ocean and the Nordic seas. CCLM is up to 4°C warmer over sea ice at the Canadian coast in comparison to ASR (Figs. 5c,d). These differences are similar in the 99th percentile and in the 95th percentile one. In the Kara Sea and Barents Sea regions, which are the main regions of interest in this study, these differences are relatively small (±1°C). The comparison of CCLM with ERA-I (Figs. 5e,f) shows smaller differences than for ASR. The region of greater differences is more pronounced in the 99th

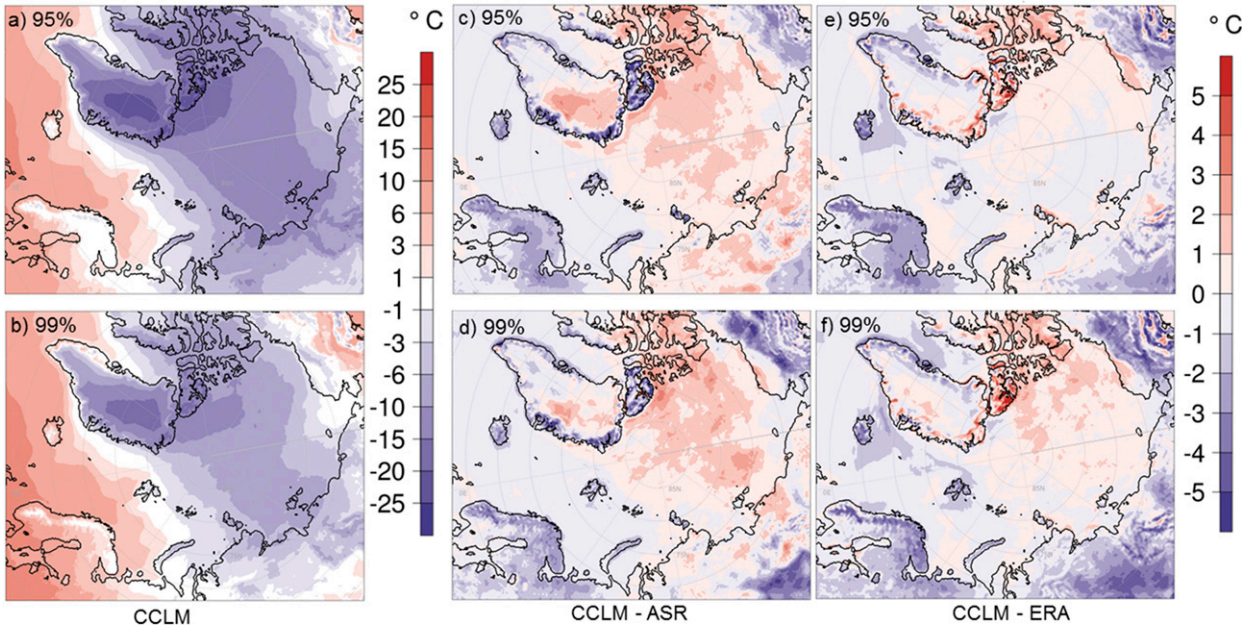

FIG. 5. (top) The 95th and (bottom) 99th percentiles of 2-m air temperature from (a),(b) CCLM; (c),(d) CCLM minus ASR; and (e),(f) CCLM minus ERA-I for the 2-m air temperature based on daily means for all winters 2002/03–2011/12.

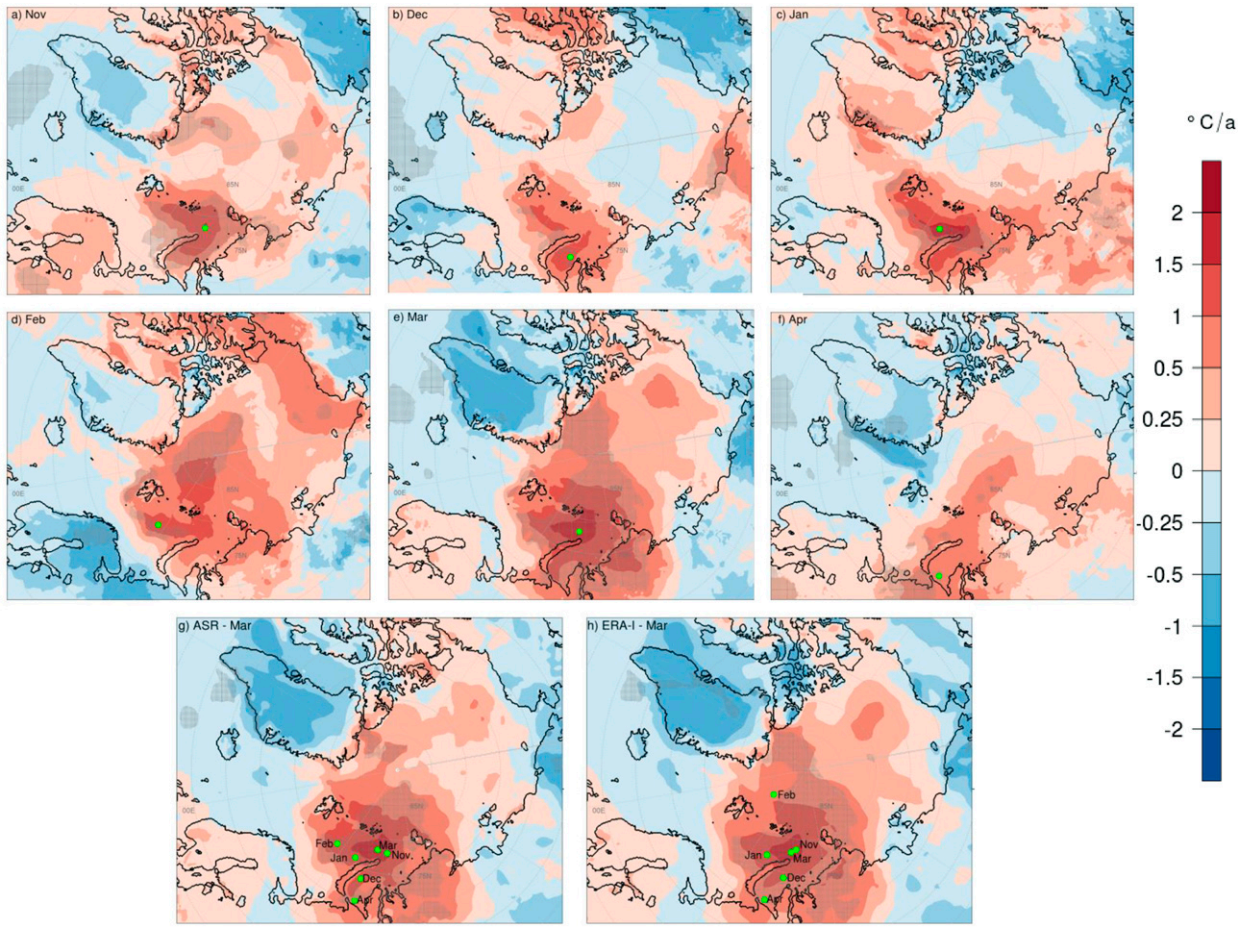

FIG. 6. (a)–(f) Spatial distribution of the trends of the 2-m air temperature (°C yr^{-1}) for CCLM monthly mean winter months for 2002/03–2011/12. Gray shaded regions indicate significance at the 95% level. Spatial trends of (g) ASR and (h) ERA-I for March 2003–12. The green dots show the region of the maximum trend for the individual months.

percentile. While CCLM minus ERA-I percentile differences are generally positive over sea ice, the opposite is found for the comparison between ASR and ERA-I (not shown). This indicates that in comparison to ERA-I, more (less) extreme warm days are present in CCLM (ASR) for the winters 2002/03–2011/12. The validation of CCLM shows only slight differences to the compared datasets including WMO stations, MODIS sea ice temperature, and ASR and ERA-I data. Thus, CCLM offers a realistic basis for the following trend analysis with slight uncertainties in the magnitudes.

4. Results: Temperature increase since 2000

a. Spatial distribution of temperature trends

The trends of the monthly mean 2-m air temperatures of CCLM are positive for all winter months since the beginning of the twenty-first century (Figs. 6a–f). By ''trend'' we mean the low-frequency variability evident in a time series of 10–16-yr duration, knowing that the climatological reference period is 30 yr. Still trend is the tendency within a certain period of time and in the following analysis the term is used as it also implies linear regression analysis. In the following we consider three different periods: 1) winter 2002/03–2011/12 because of the strongest temperature increase per decade and the overlapping data period of CCLM and ASR, 2) winter 2002/03–2014/15 because of the complete simulation period of CCLM (limited by the available AMSR sea ice information), and 3) winter 1999/2000–2015/16 using ERA-I.

From the time series in Fig. 4 it is obvious that the strongest warming occurred between 2003 and 2012 in the last two decades. Generally, the maxima of the trends are mainly located in the Kara Sea and Barents Sea region (Figs. 6a–f). Between winter 2002/03 and 2011/12 (winter period 1) the strongest trends occur in

January and, particularly March with a warming of up to 2°C yr^{-1} for March (i.e., an increase of up to 20.5°C north of Novaya Zemlya during this 10-yr period). The warming trends are generally significant at a confidence level of 95% (maximum trends even at the 99% level; not shown).

February and March also show strong nonsignificant positive trends at the Canadian coast. The ASR and ERA-I trends for March 2003–12 are shown in Figs. 6g,h. The coarser resolution of ERA-I results in smoother spatial patterns. Trends of ERA-I as well as ASR are in very good agreement with the CCLM March trend, but slightly weaker. The locations of maximum areas of the single months (green points) are similar, except for the ERA-I February location. The trend values are similar as well and have a maximum deviation of around 3°C for March between ERA-I and CCLM (Table 2). In comparison to the ERA-I changes between 1979/80 and 1999/2000 (see Fig. A1 in the appendix), the changes since 2002/03 are up to 8 times higher in the Kara Sea and Barents Sea. For the 1979/80–1999/2000 period, no consistent temperature change pattern can be found over sea ice for different winter months.

The strong 2-m air temperature increase found for 2002/03–2011/12 (winter period 1) gets weaker, if the CCLM simulations are extended to the full CCLM simulation period (2002/03–2014/15; winter period 2), but the 2-m air temperature change is still very large (Fig. 7). Figure 7 also indicates that the regions with the maximum temperature increase are all in the Barents Sea and Kara Sea. The largest temperature increase can be seen for March with 1.2°C yr^{-1} (equals 16.1°C for the 13-yr period, Table 2). December is the month with the lowest maximum 2-m air temperature increase of 0.8°C yr^{-1} (equal to 10.2°C for 13 yr). The areas of maximum 2-m air temperature increase for November, December, March, and April are located in the region north of the island Novaya Zemlya. The maximum 2-m air temperature increase for January and February takes place in the vicinity of Spitsbergen. All maximum changes are at least 95% significant (Fig. 7).

TABLE 2. Maximum 2-m air temperature increase (°C) for the ocean and sea ice area for the winter months 2002/03–2011/12 and 2002/03–2014/15. Footnotes identify the significance. Locations of the individual maximum increase are marked as green dots in Figs. 6 and 7.

	2002/03–2011/12			2002/03–2014/15
	CCLM	ASR	ERA-I	CCLM
November	16.9[a]	16.1[a]	15.1[a]	13.1[a]
December	13.9[a]	13.8[a]	12.5[a]	10.2[b]
January	18.3[a]	16.4[a]	15.9[a]	14.0[a]
February	13.3[a]	12.9[a]	11.8[a]	11.6[a]
March	20.5[a]	19.3[a]	17.3[a]	16.1[a]
April	9.9[a]	9.2[b]	8.1[a]	11.1[a]

[a] Confidence level of 99.0% and greater.
[b] Confidence level of 95.0%.

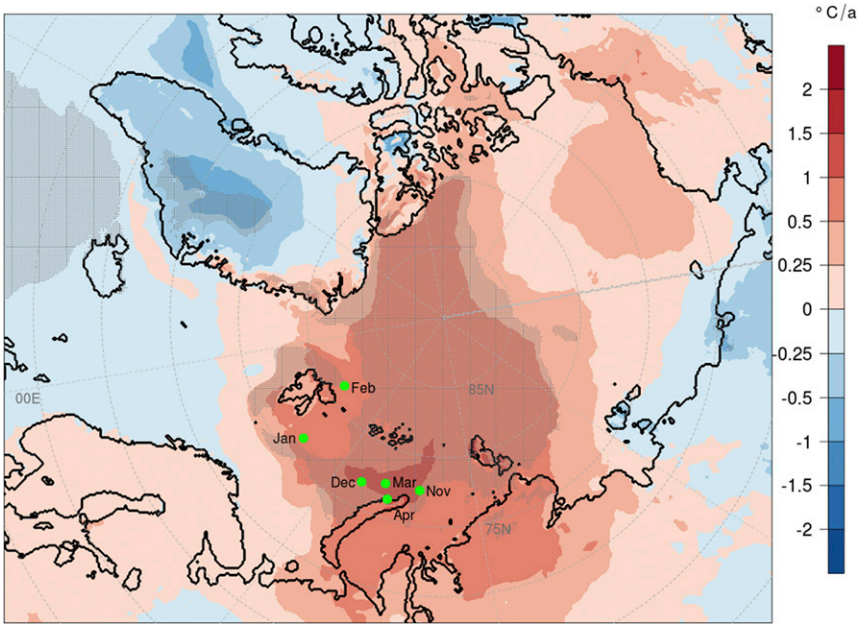

FIG. 7. Spatial distribution of the trend of the 2-m air temperature (°C yr^{-1}) for CCLM March monthly means for 2003–15 with all maximum trend regions of individual months for 2002/03–2014/15 (green). Gray shaded regions indicate significance at the 95% level.

TABLE 3. Spatially averaged 2-m air temperature mean (°C) and linear trend (°C decade^{-1}) for the ocean and sea ice area (≥70°N) for the winter periods 1979/80–1998/99, 1999/2000–2015/16, 1979/80–2015/16, 2002/03–2011/12, and 2002/03–2014/15.

	1979/80–1998/99	1999/2000–2015/16	1979/80–2015/16	2002/03–2011/12			2002/03–2014/15
	ERA-I	ERA-I	ERA-I	ERA-I	CCLM	ASR	CCLM
				Mean			
November	−17.3	−14.8	−16.1	−14.5	−15.5	−15.3	−15.6
December	−21.5	−18.7	−20.2	−18.4	−19.6	−19.2	−19.5
January	−23.2	−20.4	−21.9	−20.1	−21.2	−20.7	−21.2
February	−23.0	−21.1	−22.1	−21.0	−22.2	−21.9	−22.1
March	−21.6	−19.9	−20.8	−20.3	−21.1	−21.2	−20.7
April	−16.4	−14.2	−15.3	−13.9	−14.3	−14.7	−14.2
November–April	−20.5	−18.2	−19.4	−18.0	−19.0	−18.8	−18.9
				Trend			
November	0.8	1.7	1.3	2.3	2.6	3.1	1.3
December	−0.8	1.2	1.1	1.4	1.6	1.5	1.2
January	−0.9	2.7	1.3	1.9	2.4	1.9	0.8
February	−0.9	2.8	0.9	4.1	4.9	3.7	2.6
March	0.3	2.7	1.0	3.8	4.5	3.5	3.6
April	1.3	2.1	1.3	1.1	1.4	0.9	1.1
November–April	0.0	2.2	1.1	2.4	2.8	2.4	1.8

b. *Trends for ocean and sea ice areas*

In this section, we consider the changes in 2-m air temperature for the ocean and sea ice of the area northward of 70°N for CCLM, ASR, and ERA-I. For all months, and the time periods 1) 2002/03–2011/12, 2) 2002/03–2014/15, and 3) 1999/2000–2015/16, the 2-m air temperature increases (Table 3). The largest warming is found for February, and CCLM shows a maximum increase being about 0.8°C (1.2°C) higher than for ERA-I (ASR). The smallest trend for the complete Arctic ocean since 2002/03 occurs in April with around 1.4°C decade^{-1} for both time periods of CCLM, with 0.9°C decade^{-1} for ASR, and 1.1°C decade^{-1} for ERA-I. The maximum increase for 2002/03–2011/12 occurs in the Barents Sea and Kara Sea in March (Fig. 6), but the maximum of the area average of the ocean and the sea ice area is highest in February. The February CCLM increase is the largest with 4.9°C decade^{-1}, followed by ERA-I with 4.1°C decade^{-1}, and then ASR with 3.7°C decade^{-1}. With the exception of November, CCLM always has the largest temperature trend. The verification of CCLM and the synoptic stations showed that CCLM is slightly overestimating the 2-m air temperature in the Kara Sea and Barents Sea, except in November (section 3). This is also consistent with the percentile analysis (section 3), where CCLM has more extreme warm days (Fig. 5). The warming shown in ERA-I for January and April 1999/2000–2015/16 is stronger than for 2002/03–2011/12. The warming in February and March 2000–16 is smaller compared to February and March 2003–12, but still January, February, and March 2000–16 show a warming trend of 2.7°C decade^{-1} for the Arctic region north of 70°N. This amounts to an averaged increase of 4.5°C for the Arctic sea ice and ocean area 70°N for these months since 2000.

Comparing the CCLM trends of the two time periods, the trends per decade are smaller for the extended time period 2002/03–2014/15 (winter period 2) than for 2002/03–2011/12 (winter period 1). The difference in the trends for January and February for both time periods amounts to approximately 1.6° and 2.3°C decade^{-1}. The entire winter 2-m air temperature warming over ocean and sea ice for CCLM amounts to 2.8°C decade^{-1} for the decade 2002/03–2011/12 and 1.8°C decade^{-1} for 2002/03–2014/15. ASR and ERA-I show the same increase of 2.4°C decade^{-1} for the decade 2002/03–2011/12. For the winter period 1999/2000–2015/16 the warming trend is similar to 2002/03–2011/12 for ERA-I with 2.2°C decade^{-1}. That is 0.4°C decade^{-1} more than CCLM simulations show for 2002/03–2014/15 but 0.6°C decade^{-1} less than shown by CCLM for 2002/03–2011/12. Despite the sensitivity with respect to the chosen period, which is a result of the high interannual variability of temperature, a substantial acceleration of the temperature increase for the Arctic during the twenty-first century is documented. Spatial maps of the 2-m air temperature trends for ERA-I for the individual months of 1999/2000–2015/16 can be found in the appendix (see Fig. A2).

c. *Changes of the vertical temperature structure*

Vertical cross sections through the maximum increase area in the Kara Sea and Barents Sea during the maximum warming period (winter 2002/03–2011/12) show that the temperature increase is strongest near the surface and decreases with height (Fig. 8). The north–south

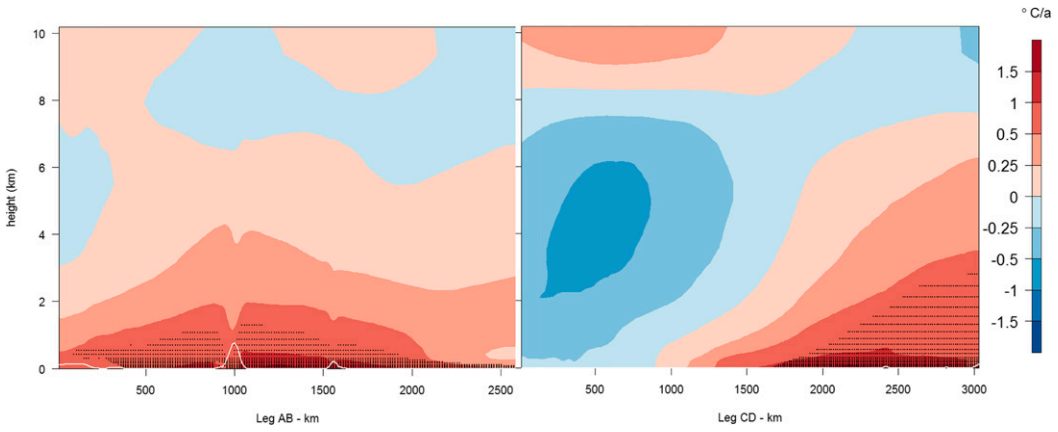

FIG. 8. Vertical cross section trends of air temperature (°C yr^{-1}) for CCLM March monthly means for 2003–12: (left) line AB, from Siberia to the North Pole and (right) line CD, from the Norwegian Sea to the Kara Sea. For the exact cross section locations see Fig. 1. White line indicates the topography.

cross section from the southern Kara Sea to the North Pole (along line AB, for exact location see Fig. 1), intersects the hot spot area of the March maximum 2-m air temperature increase in its southern part. The maximum trend of around 20.0°C decade^{-1} can only be found in the lowest layers, but a warming of up to 5°C decade^{-1} extends up to a height of 2 km. Above 2 km the trend decreases to around ±2.5°C decade^{-1}. The second cross section is orientated from the southern Norwegian Sea to the eastern Kara Sea (along line CD; see Fig. 1). It shows similar results for the Kara Sea region, but also a cooling of up to −10.1°C decade^{-1} in the Nordic seas at heights between 2 and 6 km for March 2003–12. This cooling is also present in the months February and April (not shown).

5. Discussion and conclusions

The near-surface temperature changes are temporally and spatially analyzed since the beginning of the twenty-first century. Focus lies on the three time periods: 1) winter 2002/03–2011/12 because of the strongest temperature increase per decade and the overlapping data period of the regional climate model CCLM (15-km resolution) and the reanalysis data ASR (30-km resolution), 2) winter 2002/03–2014/15 because of the complete simulation period of CCLM (limited by the available AMSR sea ice information), and 3) winter 1999/2000–2015/16 using ERA-I (79-km resolution). Spatially, the model sets identify the Barents Sea and Kara Sea area as the region with the maximum warming since 1999/2000 and especially since 2002/03. The maximum temperature increase occurring in winter is located over the ocean and therefore not captured by the synoptic observations. The quality of the CCLM results are compared with the reanalysis ASR and ERA-I, but also with synoptic observations and MODIS sea ice temperatures (not shown). CCLM agrees well with the available verification data, thus both CCLM and ASR offer a realistic basis of the presented trend analysis with slight uncertainties in the magnitudes. The comparison of CCLM with ASR shows only very slight differences over the sea ice and ocean regions. The differences are larger over the land for the 95th and 99th percentiles, where CCLM simulates higher temperatures for the extreme warm days. For the monthly mean 2-m air temperatures of the Kara Sea and Barents Sea region, CCLM shows generally larger trends and more peak values of the warming than ASR. There are minor differences in the spatial warming patterns.

The simulated warming by CCLM in the Kara Sea and Barents Sea is also compared to different ERA-I time periods. ERA-I data show a 2-m air temperature trend of less than 5°C decade^{-1} between 1979/80 and 1998/99 for the Kara Sea and Barents Sea region, while CCLM shows a warming up to 8 times higher for winter 2002/03–2014/15. The significant warming pattern in the Barents Sea was also found in other reanalysis studies (Lindsay et al. 2014; Simmons and Poli 2015). The warming from 2002/03 to 2014/15 is exceptionally high between 2002 and 2012 for the Kara Sea and Barents Sea. The maximum occurs north of Novaya Zemlya with up to 20°C for March 2003–12 and is only covered by model results. Land-based observations in the vicinity confirm the strong warming with a maximum 2-m air temperature increase of up to 15°C for March 2003–12. This is still a very strong temperature rise within such a short period of time.

The short lengths for the trend calculation result in some sensitivity of the trend magnitude with respect to the time period chosen. The comparison between the three time periods and the individual trends show the

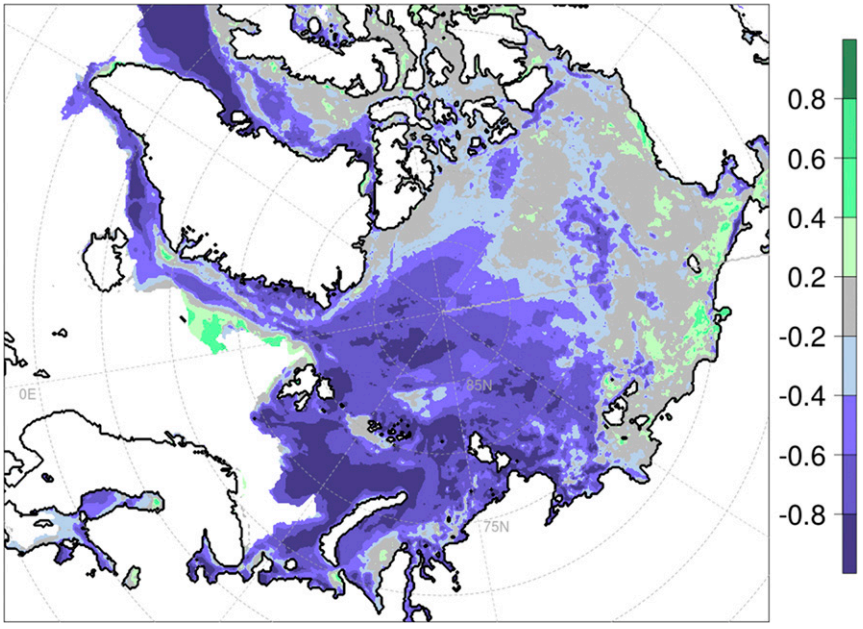

FIG. 9. Correlation of CCLM monthly mean 2-m air temperatures and AMSR-E sea ice concentration for March 2003–12.

high 2-m air temperature variability between the individual winters and therefore these calculations are not the basis for any long term trend calculations or temperature forecasts. The maximum trend in the overlapping period between ASR and CCLM starts in 2002/03 with a winter of minimum temperatures and ends in 2011/12 as a winter with maximum temperatures in the Arctic. Thus, the extension of the time period reduces the trend. Nevertheless, the air temperature rise since the beginning of the twenty-first century is clearly higher than in the previous years since records began. In addition, both observational and model data show that the temperatures in the last four winters 2013/14–2016/17 stayed more or less constant and much closer to the maximum values of the extreme warm winter 2011/12 than to any minimum winter in the recent two decades.

The sea ice decrease is the likely main reason for the warming in the Kara Sea and Barents Sea region. The vertical temperature profiles show that the warming has a maximum near the surface, but an increase of 5°C decade^{-1} is found up to 2 km. Figure 9 presents the correlation of the 2-m air temperature of CCLM and the sea ice concentration based on satellite data for March 2003–12. The negative correlation amounts up to 80% in the Kara Sea and Barents Sea region (i.e., the patterns of the sea ice decrease and the temperature rise are similar). In addition, the maximum values of 2-m air temperature for March occur in the years 2007 and 2012. These are the same years with the lowest values of recorded September Arctic sea ice concentration (Parkinson and Comiso 2013; Schröder et al. 2014). The reduced sea ice in late autumn and winter leads to an enhancement of ocean–atmosphere sensible heat flux and subsequent warming of the atmospheric boundary layer. The contribution of the heat flux to the warming depends on the seasonal cycle (Deser et al. 2010). Previous studies show that the Barents Sea plays a major role in increasing ocean–atmosphere sensible heat flux (e.g., Arthun et al. 2012; Onarheim et al. 2014; Sorokina et al. 2016) because of enhanced northward advection of warm Atlantic water, causing the extreme winter atmospheric warming found here. Changes in the frequencies of atmospheric circulation patterns partly contribute to the recent surface warming. Park et al. (2015) show that the sea ice decrease in the Barents Sea and Kara Sea region is dominated by an increase in downward infrared radiation, which is attributed to changes in the large-scale atmospheric circulations. Nevertheless, Isaksen et al. (2016) show that they play only a minor role for the observed warming around Spitzbergen, which is driven by heat exchange from the open water areas around Barents Sea and the region north of Svalbard.

This study contributes to the understanding of the spatial and temporal variability of the Arctic temperature change. It is likely that more warm winter months will follow especially in the Nordic Arctic region in future years as a result of climate change (Vikhamar-Schuler et al. 2016). Because the area with the highest trends are not covered by any observational data, high-resolution models and reanalysis data are needed together

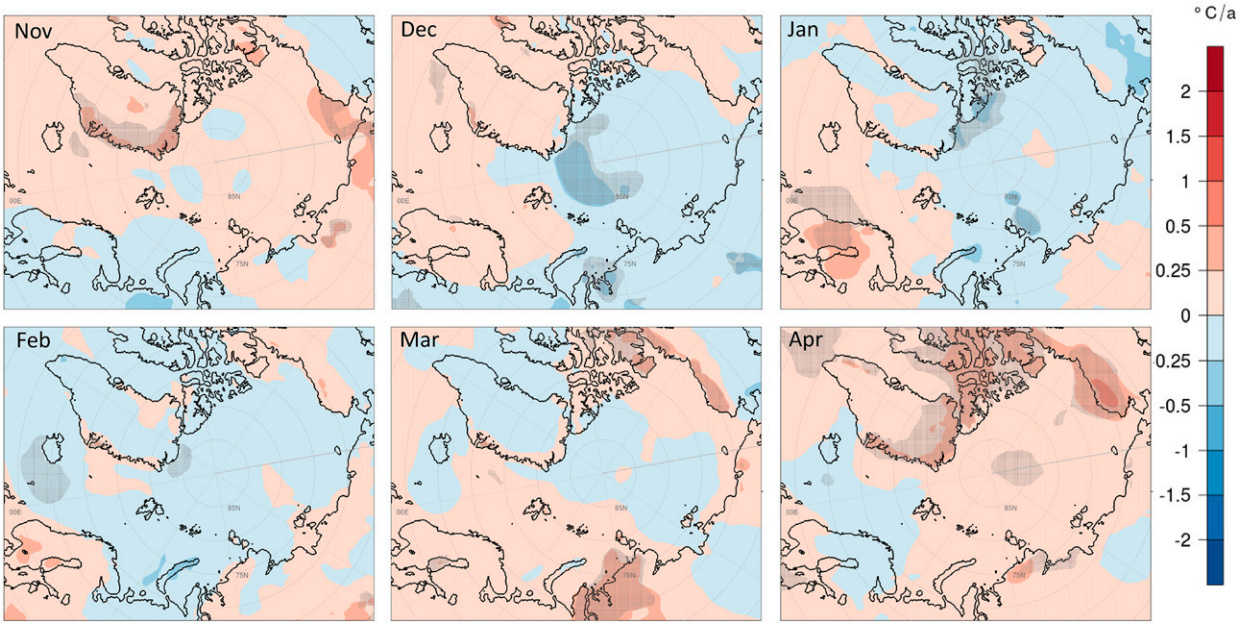

FIG. A1. Spatial distribution of the trends of the 2-m air temperature (°C yr^{-1}) for ERA-I monthly mean winter months for 1979/80–1998/99. Gray shaded regions indicate significance at the 95% level.

with improved descriptions of sea ice processes. The good agreement between CCLM and ASR encourages us to use the CCLM simulations also for a longer period in order to assess long-term trends.

Acknowledgments. This work was part of the German–Russian cooperation WTZ RUS: System Laptev Sea: TRANSDRIFT funded by the Federal Ministry of Education and Research (BMBF) under Grant 03G0833D. This work was also supported by NASA Grant NN12AI29G. The authors thank the CLM community and the German Weather Service for providing the basic COSMO-CLM Model. The AMSR-E sea ice data were provided by the University of Bremen, ERA-Interim data were provided by the ECMWF, and the PIOMAS dataset was provided by the Polar Science

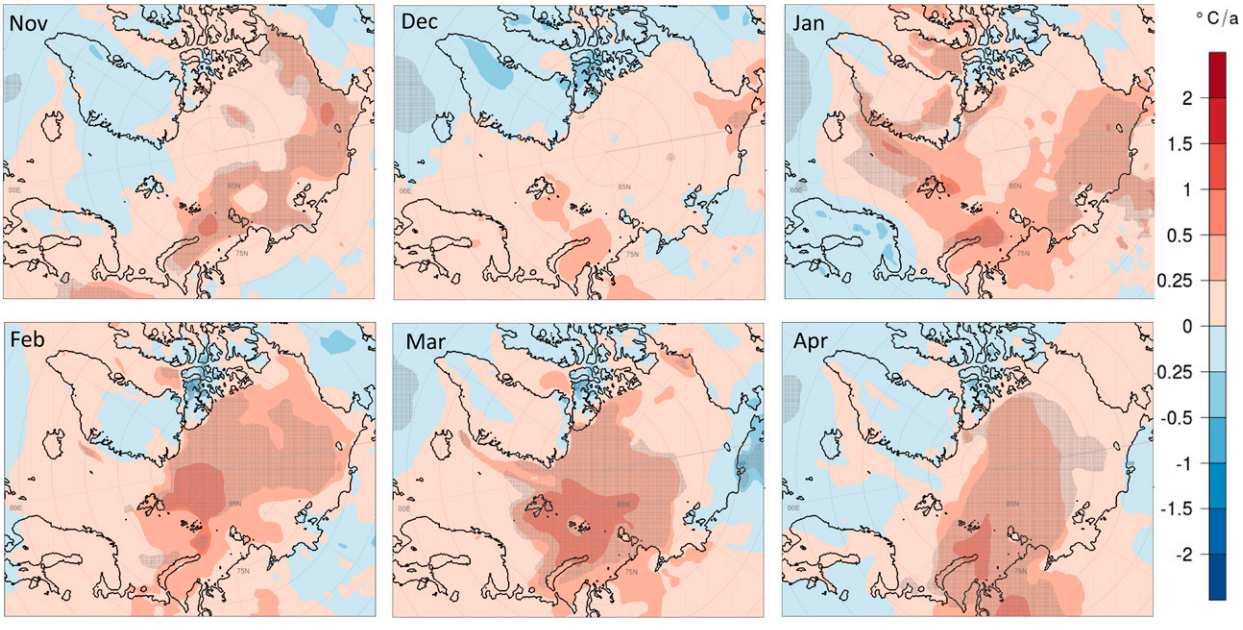

FIG. A2. As in Fig. A1, but for 1999/2000–2015/16.

Center (University of Washington). The observational data are provided by the World Meteorological Organization (WMO). We thank the DKRZ (Hamburg) for providing computational time. The German Academic Exchange Service (DAAD) funded the first author's exchange stay at the Byrd Polar and Climate Research Center, The Ohio State University. Special thanks go to Lukas Schefczyk for technical support with the CCLM. Contribution Number 1546 of Byrd Polar and Climate Research Center.

APPENDIX

Temperature Increase 1979/80–1998/99

Figure A1 shows ERA-I 2-m air temperature trends between 1979/80 and 1998/99. No consistent temperature change pattern can be found over sea ice for different months. The changes since 1999/2000 are 2–4 times higher compared to the decades before in the Kara Sea and Barents Sea (Fig. A2).

REFERENCES

Arthun, M., T. Eldevik, L. H. Smedsrud, O. Skagseth, and R. B. Ingvaldsen, 2012: Quantifying the influence of Atlantic heat on Barents Sea Ice variability and retreat. *J. Climate*, **25**, 4736–4743, doi:10.1175/JCLI-D-11-00466.1.

Bauer, M., D. Schröder, G. Heinemann, S. Willmes, and L. Ebner, 2013: Quantifying polynya ice production in the Laptev Sea with the COSMO model. *Polar Res.*, **32**, 20922, doi:10.3402/polar.v32i0.20922.

Bromwich, D. H., L. Bai, K. Hines, S. Wang, Z. Liu, H. Lin, Y. Kuo, and M. Barlage, 2012: Arctic System Reanalysis (ASR) Project. Research Data Archive at the National Center for Atmospheric Research, Computational and Information Systems Laboratory, accessed 26 May 2015, doi:10.5065/D6K072B5.

——, A. B. Wilson, L. S. Bai, G. W. K. Moore, and P. Bauer, 2016: A comparison of the regional Arctic System Reanalysis and the global ERA-Interim Reanalysis for the Arctic. *Quart. J. Roy. Meteor. Soc.*, **142**, 644–658, doi:10.1002/qj.2527.

Cohen, J., and Coauthors, 2014: Recent Arctic amplification and extreme mid-latitude weather. *Nat. Geosci.*, **7**, 627–637, doi:10.1038/ngeo2234.

Comiso, J. C., 2012: Large decadal decline of the Arctic multilayer ice cover. *J. Climate*, **25**, 1176–1193, doi:10.1175/JCLI-D-11-00113.1.

Cowtan, K., and R. G. Way, 2014: Coverage bias in the HadCRUT4 temperature series and its impact on recent temperature trends. *Quart. J. Roy. Meteor. Soc.*, **140**, 1935–1944, doi:10.1002/qj.2297.

Dee, D. P., and Coauthors, 2011: The ERA-Interim reanalysis: Configuration and performance of the data assimilation system. *Quart. J. Roy. Meteor. Soc.*, **137**, 553–597, doi:10.1002/qj.828.

Deser, C., R. Tomas, M. Alexander, and D. Lawrence, 2010: The seasonal atmospheric response to projected Arctic sea ice loss in the late twenty-first century. *J. Climate*, **23**, 333–351, doi:10.1175/2009JCLI3053.1.

Doms, G., and Coauthors, 2011: A description of the Nonhydrostatic Regional COSMO Model, Part II: Physical parametrization. Consortium for Small-Scale Modelling, Deutscher Wetterdienst, Offenbach, Germany, 161 pp., http://www.cosmo-model.org/content/model/documentation/core/cosmoPhysParamtr.pdf.

Ebner, L., D. Schröder, and G. Heinemann, 2011: Impact of Laptev Sea flaw polynyas on the atmospheric boundary layer and ice production using idealized mesoscale simulations. *Polar Res.*, **30**, 7210, doi:10.3402/polar.v30i0.7210.

Francis, J. A., and E. Hunter, 2006: New insight into the disappearing Arctic sea ice. *Eos, Trans. Amer. Geophys. Union*, **87**, 509–524, doi:10.1029/2006EO460001.

Gillett, N. P., D. A. Stone, P. A. Stott, T. Nozawa, A. Y. Karpechko, G. C. Heger, M. F. Wehner, and P. D. Jones, 2008: Attribution of polar warming to human influence. *Nat. Geosci.*, **1**, 750–754, doi:10.1038/ngeo338.

Graversen, R. G., and M. Wang, 2009: Polar amplification in a coupled climate model with locked albedo. *Climate Dyn.*, **33**, 629–643, doi:10.1007/s00382-009-0535-6.

——, T. Mauritsen, M. Tjernstrom, E. Kallen, and G. Svensson, 2008: Vertical structure of recent Arctic warming. *Nature*, **451**, 53–56, doi:10.1038/nature06502.

Gutjahr, O., G. Heinemann, A. Preusser, S. Willmes, and C. Drüe, 2016: Quantification of ice production in Laptev Sea polynyas and its sensitivity to thin-ice parameterizations in a regional climate model. *Cryosphere*, **10**, 2999–3019, doi:10.5194/tc-10-2999-2016.

Hall, D., J. Key, K. Casey, G. Riggs, and D. Cavalieri, 2004: Sea ice surface temperature product from MODIS. *IEEE Trans. Geosci. Remote Sens.*, **42**, 1076–1087, doi:10.1109/TGRS.2004.825587.

IPCC, 2013: *Climate Change 2013: The Physical Science Basis*. Cambridge University Press, 1535 pp., doi:10.1017/CBO9781107415324.

Isaksen, K., O. Nordli, E. Forland, E. Lupikasza, S. Eastwood, and T. Niedzwiedz, 2016: Recent warming on Spitsbergen—Influence of atmospheric circulation and sea ice cover. *J. Geophys. Res. Atmos.*, **121**, 11 913–11 931, doi:10.1002/2016JD025606.

Koltzow, M., 2007: The effect of a new snow and sea ice albedo scheme on regional climate model simulations. *J. Geophys. Res.*, **112**, D07110, doi:10.1029/2006JD007693.

Lindsay, R. W., J. Zhang, A. J. Schweiger, M. A. Steele, and H. Stern, 2009: Arctic sea ice retreat in 2007 follows thinning trend. *J. Climate*, **22**, 165–176, doi:10.1175/2008JCLI2521.1.

——, M. Wensnahan, A. Schweiger, and J. Zhang, 2014: Evaluation of seven different atmospheric reanalysis products in the Arctic. *J. Climate*, **27**, 2588–2606, doi:10.1175/JCLI-D-13-00014.1.

Moore, G. W. K., 2013: The Novaya Zemlya Bora and its impact on Barents Sea air-sea interaction. *Geophys. Res. Lett.*, **40**, 3462–3467, doi:10.1002/grl.50641.

——, I. A. Renfrew, B. E. Harden, and S. H. Mernild, 2015: The impact of resolution on the representation of southeast Greenland barrier winds and katabatic flows. *Geophys. Res. Lett.*, **42**, 3011–3018, doi:10.1002/2015GL063550.

——, D. H. Bromwich, A. B. Wilson, I. A. Renfrew, and L. Bai, 2016: Arctic System Reanalysis improvements in topographically-forced winds near Greenland. *Quart. J. Roy. Meteor. Soc.*, **142**, 2033–2045, doi:10.1002/qj.2798.

Notz, D., and J. Marotzke, 2012: Observations reveal external driver for Arctic sea-ice retreat. *Geophys. Res. Lett.*, **39**, L08502, doi:10.1029/2012GL051094.

Onarheim, I. H., L. H. Smedsrud, R. B. Ingvaldsen, and F. Nilsen, 2014: Loss of sea ice during winter north of Svalbard. *Tellus*, **66A**, 23933, doi:10.3402/tellusa.v66.23933.

Overland, J. E., and M. Wang, 2010: Large-scale atmospheric circulation changes are associated with the recent loss of Arctic sea ice. *Tellus*, **62A**, 1–9, doi:10.1111/j.1600-0870.2009.00421.x.

Park, D. S. R., S. Lee, and S. B. Feldstein, 2015: Attribution of the recent winter sea ice decline over the Atlantic sector of the Arctic Ocean. *J. Climate*, **28**, 4027–4033, doi:10.1175/JCLI-D-15-0042.1.

Parkinson, C. L., and J. C. Comiso, 2013: On the 2012 record low Arctic sea ice cover: Combined impact of preconditioning and an August storm. *Geophys. Res. Lett.*, **40**, 1356–1361, doi:10.1002/grl.50349.

Pithan, F., and T. Mauritsen, 2014: Arctic amplification dominated by temperature feedbacks in contemporary climate models. *Nat. Geosci.*, **7**, 181–184, doi:10.1038/ngeo2071.

Preußer, A., G. Heinemann, S. Willmes, and S. Paul, 2016: Circumpolar polynya regions and ice production in the Arctic: Results from MODIS thermal infrared imagery for 2002/2003 to 2014/2015 with a regional focus on the Laptev Sea. *Cryosphere*, **10**, 3021–3042, doi:10.5194/tc-10-3021-2016.

Rockel, B., A. Will, and A. Hense, 2008: The Regional Climate Model COSMO-CLM (CCLM). *Meteor. Z.*, **17**, 347–348, doi:10.1127/0941-2948/2008/0309.

Schröder, D., G. Heinemann, and S. Willmes, 2011: The impact of a thermodynamic sea-ice module in the COSMO numerical weather prediction model on simulations for the Laptev Sea, Siberian Arctic. *Polar Res.*, **30**, 6334, doi:10.3402/polar.v30i0.6334.

——, D. L. Feltham, D. Flocco, and M. Tsamados, 2014: September Arctic sea-ice minimum predicted by spring melt-pond fraction. *Nat. Climate Change*, **4**, 353–357, doi:10.1038/nclimate2203.

Screen, J. A., and I. Simmonds, 2010: The central role of diminishing sea ice in recent Arctic temperature amplification. *Nature*, **464**, 1334–1337, doi:10.1038/nature09051.

——, C. Deser, and I. Simmonds, 2012: Local and remote controls on observed Arctic warming. *Geophys. Res. Lett.*, **39**, L10709, doi:10.1029/2012GL051598.

Serreze, M. C., and J. A. Francis, 2006: The Arctic amplification debate. *Climatic Change*, **76**, 241–264, doi:10.1007/s10584-005-9017-y.

——, and R. G. Barry, 2011: Processes and impacts of Arctic amplification: A research synthesis. *Global Planet. Change*, **77**, 85–96, doi:10.1016/j.gloplacha.2011.03.004.

——, A. P. Barrett, J. C. Stroeve, D. M. Kindig, and M. M. Holland, 2009: The emergence of surface-based Arctic amplification. *Cryosphere*, **3**, 11–19, doi:10.5194/tc-3-11-2009.

Shindell, D., and G. Faluvegi, 2009: Climate response to regional radiative forcing during the twentieth century. *Nat. Geosci.*, **2**, 294–300, doi:10.1038/ngeo473.

Simmons, A. J., and P. Poli, 2015: Arctic warming in ERA-Interim and other analyses. *Quart. J. Roy. Meteor. Soc.*, **141**, 1147–1162, doi:10.1002/qj.2422.

Smirnova, J., and P. Golubkin, 2017: Comparing polar lows in atmospheric reanalyses: Arctic System Reanalysis versus ERA-Interim. *Mon. Wea. Rev.*, **145**, 2375–2383, doi:10.1175/MWR-D-16-0333.1.

Sorokina, S. A., C. Li, J. J. Wettstein, and N. G. Kvamsto, 2016: Observed atmospheric coupling between Barents Sea ice and the warm-Arctic cold-Siberian anomaly pattern. *J. Climate*, **29**, 495–511, doi:10.1175/JCLI-D-15-0046.1.

Spreen, G., L. Kaleschke, and G. Heygster, 2008: Sea ice remote sensing using AMSR-E 89-GHz channels. *J. Geophys. Res.*, **113**, C02S03, doi:10.1029/2005JC003384.

Steppeler, J., G. Doms, U. Schättler, H. W. Bitzer, A. Gassmann, U. Damrath, and G. Gregoric, 2003: Meso-gamma scale forecasts using the nonhydrostatic model LM. *Meteor. Atmos. Phys.*, **82**, 75–96, doi:10.1007/s00703-001-0592-9.

Stroeve, J. C., M. C. Serreze, M. M. Holland, J. E. Kay, J. Malanik, and A. P. Barrett, 2012: The Arctic's rapidly shrinking sea ice cover: A research synthesis. *Climatic Change*, **110**, 1005–1027, doi:10.1007/s10584-011-0101-1.

Tilinina, N., S. K. Gulev, and D. H. Bromwich, 2014: New view of Arctic cyclone activity from the Arctic System Reanalysis. *Geophys. Res. Lett.*, **41**, 1766–1772, doi:10.1002/2013GL058924.

Vikhamar-Schuler, D., K. Isaksen, J. E. Haugen, H. Tommervik, B. Luks, T. Vikhamar-Schuler, and J. W. Bjerke, 2016: Changes in winter warming events in the Nordic Arctic region. *J. Climate*, **29**, 6223–6244, doi:10.1175/JCLI-D-15-0763.1.

Wesslen, C., M. Tjernstroem, D. H. Bromwich, G. Boer, A. M. L. Ekman, L. Bai, and S. H. Wang, 2014: The Arctic summer atmosphere: An evaluation of reanalyses using ASCOS data. *Atmos. Chem. Phys.*, **14**, 2605–2624, doi:10.5194/acp-14-2605-2014.

Winton, M., 2006: Amplified Arctic climate change: What does surface albedo feedback have to do with it? *Geophys. Res. Lett.*, **33**, L03701, doi:10.1029/2005GL025244.

Zhang, J., and D. A. Rothrock, 2003: Modeling global sea ice with a thickness and enthalpy distribution model in generalized curvilinear coordinates. *Mon. Wea. Rev.*, **131**, 845–861, doi:10.1175/1520-0493(2003)131<0845:MGSIWA>2.0.CO;2.